Soliton trapping in a disordered lattice

Zhi-Yuan Sun, Shmuel Fishman, and Avy Soffer

Phys. Rev. E **92**, 012901 — Published 1 July 2015

DOI: 10.1103/PhysRevE.92.012901

Soliton Trapping in Disordered Lattice

Zhi-Yuan Sun*, Shmuel Fishman†
Department of Physics,
Technion-Israel Institute of Technology, Haifa 32000, Israel

Avy Soffer‡
Department of Mathematics,
Rutgers University, New Jersey 08854, U.S.A

June 11, 2015

Abstract

In recent years, the competition between randomness and nonlinearity was extensively explored. In the present paper, dynamics of solitons of the Ablowitz-Ladik model in the presence of a random potential is studied. In absence of the random potential it is an integrable model and the solitons are stable. As a result of the random potential this stability is destroyed. In some regime, for short times particle-like dynamics with constant mass is found. There is another regime, where particle-like dynamics with varying mass takes place. In particular an effective potential is found. It predicts correctly changes in the direction of motion of the soliton. This potential is a scaling function of time and strength of the potential, leading to a relation between the first time when the soliton changes direction and the strength of the random potential.

PACS number(s): 05.45.Yv, 42.65.Tg

Keywords: Ablowitz-Ladik model; random potential; soliton trapping; particle approach

*with e-mail address as sunzhiyuan137@aliyun.com
†with e-mail address as fishman@physics.technion.ac.il
‡with e-mail address as soffer@math.rutgers.edu

I. INTRODUCTION

Solitons are one of the most remarkable manifestations of nonlinearity. They are found for continuous systems for the Nonlinear Schrödinger Equation (NLSE) in one dimension (1D) [1]. On the lattice mobile solitons are found for the model introduced by Ablowitz and Ladik (AL) [2], while for the ordinary NLSE on a lattice, a mobile soliton is only an approximate concept. Both on a lattice and in the continuum disorder tends to affect and typically destroy solitons. In the present work this will be studied for a 1D lattice in the framework of the AL model.

For the continuous system, early numerical work of Bronski [3] indicates that, a NLSE soliton becomes trapped in the random media when its kinetic energy decreases sufficiently and is of comparable size to the background potential. Akkermans et.al. [4] numerically show that a soliton bounces back and forth between high potential barriers in attractive Bose-Einstein condensates in the framework of the Gross-Pitaevskii Equation with strong disorder. In addition, like the Anderson localization of linear waves in random media, some authors relate the localization of solitons in disordered environment to *Anderson localization* [5, 6].

In absence of a random potential the AL model is

$$i\frac{\partial\psi_n}{\partial t} = -(\psi_{n-1} + \psi_{n+1})(1 + |\psi_n|^2) \ , \tag{1}$$

where ψ_n is the wavefunction on site n at time t. The AL model is an integrable discrete version of the continuous NLSE, while the discrete version of the ordinary NLSE is nonintegrable. This relates the AL model to many physical systems, for instance, in the nonlinear waveguide arrays [7, 8] and discrete molecular chains [9, 10]. The integrability of the AL model is manifested by the existence of a mobile soliton solution [11, 12]

$$\psi_n(t) = \frac{\sinh(\mu)}{\cosh[\mu(n-x)]}\exp[ik(n-x) + i\alpha] \ , \tag{2}$$

where the time-dependent parameters x and α can be expressed as

$$\dot{x} = 2\frac{\sinh(\mu)}{\mu}\sin(k) \ , \tag{3a}$$

$$\dot{\alpha} = 2[\cosh(\mu)\cos(k) + \frac{k}{\mu}\sinh(\mu)\sin(k)] \ . \tag{3b}$$

From (2) we see that $\frac{1}{\mu}$ characterizes the width of the soliton and x is its center. On the other hand, the AL equation has two conserved quantities, the first of which can be defined as the mass of the soliton solution [11–13]

$$M_s = \sum_{n=-\infty}^{\infty} \ln(1 + |\psi_n|^2) \ , \tag{4}$$

while the second can be defined as the momentum of the motion [11–13]

$$P = i\sum_{n=-\infty}^{\infty} (\psi_n\psi_{n+1}^* - \psi_n^*\psi_{n+1}) \ , \tag{5}$$

where $*$ denotes the complex conjugation. For the soliton solution (2) we can calculate that (also can see Appendix of [11])

$$M_s = 2\mu \ , \tag{6}$$

and

$$P = M_s \dot{x} = 4\sinh(\mu)\sin(k) \ . \tag{7}$$

Therefore M_s can be indeed considered as the mass of the soliton.

In the present work we will study solitons for the AL model with a random potential defined by

$$i\frac{\partial \psi_n}{\partial t} = -(\psi_{n-1} + \psi_{n+1})(1 + |\psi_n|^2) + \varepsilon_n \psi_n \ , \tag{8}$$

where ε_n are independent random variables uniformly distributed in the interval $[-\frac{W}{2}, \frac{W}{2}]$. This is the disordered version of (1). The disordered NLSE,

$$i\frac{\partial \psi_n}{\partial t} = -(\psi_{n-1} + \psi_{n+1}) + \varepsilon_n \psi_n + \beta|\psi_n|^2\psi_n \ , \tag{9}$$

is a paradigm for the exploration of the competition between effects of disorder that are tending to localize and the ones of nonlinearity that are tending to enhance spreading (for a review see [14]). Most of the work on (9) addressed this conceptional problem. It was motivated by the exploration of transport in optical waveguides, where a component of the electric field plays the role of the wave function [8], and by dynamics of cold atoms in disordered potentials [15]. The hope is that many qualitative results obtained in the framework of (8) will hold also for (9). In the exploration of (8) we can take advantage of the fact that in absence of disorder it reduces to (1) that is integrable.

For the continuous version, two early reviews [16, 17] have addressed the propagation of solitons in disordered systems; in the works by Bronski [3, 18] and Garnier [19], they show two regimes for the NLSE soliton propagation. In one regime, the soliton mass decays while its velocity approaches a constant; in the other regime, the soliton mass approaches a constant while its velocity decays very slowly. Garnier further applied a perturbation theory of the inverse scattering transform to confirm that similar two regimes are found for the AL solitons with on-site random potential (in the limit of zero randomness) [20]. Which regime is relevant depends on the value of the initial mass of the AL soliton. For large μ, the mass approaches a constant, while for small μ, the velocity approaches a constant.

However, we will show numerically, for the weak randomness, that the large soliton will be trapped before its velocity decreases to zero. Additionally, we will find a regime in which the AL soliton has possibility to be accelerated on the average by the specific randomness. We will also characterize the regime where soliton can be trapped by the disorder using a particle approach, namely, where the soliton can be considered as a particle.

The outline of the paper is as follows. In Section II the dynamics is classified by the initial value of the soliton mass. In Section III a regime where the soliton can be considered as particle

is studied, and in Section IV a scaling dependence of the time when the soliton is trapped is found to scale with the strength of the random potential W. The results are summarized in Section V.

II. SOLITON PROPAGATION IN A DISORDERED LATTICE

In this section we will study the solution of Eq. (8) numerically and semianalytically in order to develop an intuitive picture of the soliton dynamics. The initial soliton is the one found for a chain without disorder, given by (2) with

$$x = 0, \quad \dot{x} > 0 \ , \tag{10a}$$

$$M_s(t=0) = 2\mu_0 \ , \tag{10b}$$

$$\mu_0 = \mu(t=0) \ . \tag{10c}$$

The numerical solution is obtained propagating the soliton by Eq. (8). To save computer resources we use a coordinate system moving with the center of mass of the soliton, consisting of N sites, centered on soliton. The computation is performed using a 4th-order Runge-Kutta type algorithm in time, and an absorbing-wave boundary condition. In Appendix C the validity of the method for the parameters used is verified. We define the following quantities:

soliton mass

$$M_s^{(N)} = \sum_n^N \ln(1+|\psi_n|^2) \ ; \tag{11}$$

center of mass coordinate

$$x^{(N)} = \sum_n^N n \ln(1+|\psi_n|^2)/M_s^{(N)} \ , \tag{12}$$

and the second moment

$$m_2^{(N)} = \sum_n^N (n-x^{(N)})^2 \ln(1+|\psi_n|^2) \ , \tag{13}$$

while the soliton velocity is

$$v = \Delta x^{(N)}/\Delta t \ , \tag{14}$$

where $\Delta x^{(N)}$ is the change of $x^{(N)}$ during the time interval Δt (here we use $\Delta t = 0.001$). In addition, two parameters, that characterize the soliton are introduced in the simulation: one is the amplitude of the soliton

$$A_s = \max_n |\psi_n|^2 \ , \tag{15}$$

the other one is the soliton width, defined as the minimum N_w satisfying

$$\sum_{-(N_w-1)/2}^{(N_w-1)/2} \ln(1+|\psi_n|^2)/M_s^{(N)} \geq 1-\delta \ , \tag{16}$$

here $\delta = 0.01$ [note that, in simulation we first find the peak position of the soliton, then (16) is calculated with this position as the center].

There are basically 3 regimes characterized by the initial value of μ:

$$(A) \quad \mu_0 \gg 1 \; ; \tag{17a}$$

$$(B) \quad \mu_0 \approx 1 \; ; \tag{17b}$$

$$(C) \quad \mu_0 \ll 1 \; . \tag{17c}$$

A. The regime $\mu_0 \gg 1$

We choose an AL soliton with $\mu_0 = 3$, which has more than 99% mass concentrating in 3 lattice sites ($N_w = 3$). The reason for picking up a soliton of such narrow width is based on the fact that it is compact enough to admit low level of mass radiation resulting of randomness. Such low-level radiation is necessary for observing possible soliton acceleration in our numerical simulation. The initial velocity of the soliton is chosen as $\dot{x}(t = 0) = 1$, and one specific realization of the random potential with $W = 0.1$ is used. Note that $0.04 \lesssim W \lesssim 0.1$ can be seen as the weak randomness in our discussion. However if randomness is very weak, the soliton dynamics may not be distinguished from the one in the limit of zero randomness as in [20].

Assuming the random potential is a perturbation, the approximate equations for the various parameters in this potential can be derived following the work of Cai et.al. [11]. The resulting equations derived in Appendix A are

$$\dot{\mu} = 0 \; , \tag{18a}$$

$$\dot{x} = \frac{2\sinh(\mu)}{\mu}\sin(k) \; , \tag{18b}$$

$$\dot{k} = -\sinh^2(\mu) \sum_{n=-\infty}^{+\infty} \frac{\varepsilon_n \tanh[\mu(n-x)]}{\cosh[\mu(n+1-x)]\cosh[\mu(n-1-x)]} \; , \tag{18c}$$

$$\begin{aligned} \dot{\alpha} = {} & 2[\cosh(\mu)\cos(k) + \frac{k}{\mu}\sinh(\mu)\sin(k)] \\ & + \sinh^2(\mu) \sum_{n=-\infty}^{+\infty} \frac{\varepsilon_n (n-x)\tanh[\mu(n-x)]}{\cosh[\mu(n+1-x)]\cosh[\mu(n-1-x)]} \\ & - \sinh(\mu)\cosh(\mu) \sum_{n=-\infty}^{+\infty} \frac{\varepsilon_n}{\cosh[\mu(n+1-x)]\cosh[\mu(n-1-x)]} \; . \end{aligned} \tag{18d}$$

Eqs. (18) are integrated numerically with the initial conditions (10). The algorithm used is the 4th-order Runge-Kutta with $\Delta t = 0.001$, and the summations are truncated to a finite window around the center of mass of the soliton. The values of the parameters μ, k, x, and α are inserted in (2). We refer to this solution as the semianalytical solution. We compare this solution with the numerical integration of Eq. (8) (referred as the numerical solution), and the results are presented in Fig. 1. In Fig. 1(a) we compare the center of mass coordinate x of (2) and (12) found in the semianalytical calculation with the numerical solution. It is found

that on the average the velocity of the semianalytical solution is somewhat larger than the one found numerically. In Fig. 1(b) the velocity of the center of mass and the second moment are presented. The plots for the velocity are zoomed in Figs. 1(c)-(e), and the soliton profiles are shown in Fig. 1(f). We note that for $t < 100$ there is excellent agreement between the numerical and the semianalytical results. At the time $t > 100$ the second moment increases rapidly, therefore the approximation (18) is not justified anymore, and large deviation between the two solutions are shown.

B. The regime $\mu_0 \approx 1$

As a representative example in this regime, we study a soliton with $\mu_0 = 1$, moving in one realization of the random potential with $W = 0.1$. We solve numerically Eq. (8) with the initial condition (10). In this case the initial width of the soliton is 7 sites ($N_w = 7$). The results are presented in Fig. 2. We find that the center of mass x moves monotonically to the right till a time $t = T_c$ when oscillations start [see Fig. 2(a)]. From Fig. 2(b) we see that the velocity decreases monotonically for $t < T_c$ and oscillates for $t > T_c$. The period of these oscillations decreases with time. From Fig. 2(c) we see that the mass decreases with time and in the first stage this decrease is rapid, therefore the approximation (18) fails. Finally the mass approaches a nonvanishing constant. Fig. 2(d) presents the soliton profiles. The interesting phenomenon we find is the trapping of the soliton for $t > T_c$ as a result of randomness. Such trapping is a general soliton behavior, and it is not specific to any realization of randomness, as we tested explicitly. In Fig. 2(e), we show the averaged soliton velocity $v^{(av)}$ and mass $M_s^{(av)}$, over 12 realizations of the random potential. The general features are similar to the ones found for specific realizations, but the oscillations in Fig. 2(b) are washed out by the averaging. The particle aspect of this dynamics in this regime will be discussed in the next section.

C. The regime $\mu_0 \ll 1$

In this regime, the soliton has a larger width, and it is easier to loose its mass through radiation. With a limit of zero randomness, Garnier [20] shows that the soliton propagates with its mass decreasing to zero, and its velocity to a nonvanishing constant. In fact, the radiation induces a remarkable deformation on the soliton profile after some time of propagation if the randomness is not weak enough. In Fig. 3 we present an example with $\mu_0 = 0.5$ [where the initial width of the soliton is 11 sites ($N_w = 11$)] and $W = 0.1$. The initial condition is (10). From Fig. 3(a) we see that the soliton spreads, and radiates its mass over 300 sites in the time $t = 1000$. From Figs. 3(b) and (c) we conclude that the mass and velocity decrease. Such decrease of velocity includes some short time intervals where the velocity oscillates approximately near a constant. The similar time intervals have been observed in the work of Franzosi et.al. [21], as they studied the mobile discrete breathers propagating on very weak backgrounds in the framework of discrete NLSE. Their time intervals appear to be much longer, with weaker velocity oscillations, since their background perturbation is very weak. Similar qualitative be-

havior was found for different realizations of the random potential. Moreover, Fig. 3(d) shows the averaged soliton velocity and mass over 12 realizations of random potentials. We have not observed the trapping behavior in this regime, especially before the soliton undergoes a large deformation.

III. PARTICLE APPROACH FOR SOLITON TRAPPING IN DISORDERED AL LATTICE

In this section we will study the question: Can an AL soliton in a weak random potential be considered as particle?

We will focus on the soliton trapping in the second regime where $\mu_0 \approx 1$, and try to give a particle description of the trapping behavior. We start from the momentum (5), and assume it still to be the momentum for the model (8) when the random potential is weak. Taking a derivative on both sides of Eq. (5) with respect to t, and substituting Eq. (8) into the result, we can obtain

$$\frac{dP}{dt} = 2 \sum_{n=-\infty}^{+\infty} \mathrm{Re}(\psi_n \psi_{n+1}^*)(\varepsilon_n - \varepsilon_{n+1}) \ , \tag{19}$$

where Re means the real part. For derivation see Appendix B. With the assumption that the soliton is particle-like, Eq. (19) can be viewed as the variation rate of its momentum. On the other hand, dP/dt by (7) can be also written as

$$\frac{dP}{dt} = \frac{dM_s}{dt} v + M_s \frac{d^2x}{dt^2} \ . \tag{20}$$

Notice that, due to the mass radiation, the term dM_s/dt in Eq. (20) can not be neglected, especially before soliton trapping. Therefore, we can write the randomness-generated *force* in two ways, one is directly

$$F_1 = M_s \frac{d^2x}{dt^2} \ , \tag{21}$$

using (19) and (20) we derive

$$F_2 = 2 \sum_{n=-\infty}^{+\infty} \mathrm{Re}(\psi_n \psi_{n+1}^*)(\varepsilon_n - \varepsilon_{n+1}) - \frac{dM_s}{dt} v \ . \tag{22}$$

The test of the particle-like picture is performed by comparing the forces F_1 and F_2 presented in Fig. 4. Excellent agreement is found. These results strongly support the description of solitons as particles. In this picture with the force F_2 we associate work done on the soliton that decreases its kinetic energy with an effective potential

$$U(t) = U_0 - \int_{t_0}^{t} F_2 v dt' \ , \tag{23}$$

where U_0 is a parameter which can be viewed as the initial energy to be determined as the constant that leads the mean of U, over the time interval of trapping in simulations, to be

zero, i.e., $U_0 =< \int_{t>T_c} F_2 v dt >$. With the same data, we plot both of this effective potential $U(t)$ and soliton velocity in Fig. 4(e). It shows that the first reflection ($T_c \approx 1100$), with the soliton velocity changing its sign, occurs at a peak position of the effective potential. Also other changes in the direction of motion of the soliton take place at maxima of $U(t)$ as can be seen from Fig. 4(e). This is a direct result of (23) since

$$\frac{dU(t)}{dt} = -vF_2 \ , \tag{24}$$

therefore $\frac{dU(t)}{dt} = 0$ implies either $F_2 = 0$ or $v = 0$.

We note that for $t > T_c$ the soliton is trapped and oscillates in space. This is localization that can be described completely classically, as it results of a potential. Therefore it differs from the Anderson localization of solitons claimed in earlier works [6, 22, 23]. Sacha et.al. [6, 23] studied a quasi-one-dimensional bright matter-wave soliton, in a spatially correlated disordered potential. They find the soliton shape is hardly affected when the potential is weak and smooth, but the quantum motion of the soliton's center-of-mass displays Anderson localization. The similar investigation on dark solitons was performed by Mochol et.al. [22]. Our case is completely classical. It constitutes of two stages: one is for $t < T_c$, where the soliton propagates losing its mass and kinetic energy, however, the kinetic energy is still much larger than the random potential (as we checked explicitly); the other one is for $t > T_c$, where the soliton is trapped and localized by the randomness, with its kinetic energy comparable to the random potential. Both stages can be described using a particle with varying mass moving in an effective random potential, as shown in Sec. III.

IV. SCALING OF THE TRAPPING TIME T_c

In this section we demonstrate that there exists a scaling relation between the time T_c when the trapping starts and the random potential strength W. In Figs. 5(a) and (b) T_c is plotted as a function of W. It is found that

$$T_c \sim W^{-\eta} \ , \tag{25}$$

with $\eta = 2.32 \pm 0.41$. For each $W \in [0.06, 0.1]$, we average the function $U(t)$ of (23) over 6 different realizations to derive $U^{(av)}(t)$, and plot it till the minimum value of T_c of 6 realizations in Fig. 5(c). From Fig. 5(d), we see that $U^{(av)}$ is related to W and t via the combination tW^2. This suggests the scaling relation

$$U^{(av)} \approx \Gamma(tW^2) \ , \tag{26}$$

where Γ is the scaling function. If trapping starts at the same value of Γ, one finds

$$T_c \propto W^{-2} \ . \tag{27}$$

Here we want to make some comments on T_c. In the calculation of (25), we use one realization of random numbers uniformly distributed in $[-1, 1]$, but multiplied by the strength

$W/2$, as the random potential. Since the change of T_c is obvious for small variation of W [see Figs. 5(a) and (b)], it can generally reflect the scaling relation. In the following, we will use multiple realizations of random potentials, in the statistical sense, to briefly study the trapping of solitons in the regime $t > T_c$.

The time T_c can be viewed as a time when the soliton enters the trapping regime, and it should relate to the classical localization. We define the following quantity $\widetilde{x}$ for any realization of the random potential,

$$\widetilde{x} = \frac{1}{T_\infty - T_c} \int_{T_c}^{T_\infty} x(t) dt \ , \tag{28}$$

where T_∞ is the upper boundary of time in numerical simulation. Therefore, for each W, we can derive the statistical averaging $T_c^{(av)} = \langle T_c \rangle$ and $x^{(av)} = \langle \widetilde{x} \rangle$, as well as its standard derivation $\sigma_x = [\langle (\widetilde{x} - x^{(av)})^2 \rangle]^{1/2}$, where $\langle \cdot \rangle$ is the averaging over realizations of random potential. These averaged parameters provide information about the localization of solitons. We carried out the average over 250 realizations of random potentials for each W, with the results shown in Fig. 6, and found these parameters scale with W as

$$T_c^{(av)} \sim W^{-\eta_1} \quad \eta_1 = 2.46 \pm 0.04 \ , \tag{29a}$$

$$x^{(av)} \sim W^{-\eta_2} \quad \eta_2 = 2.27 \pm 0.04 \ , \tag{29b}$$

$$\sigma_x \sim W^{-\eta_3} \quad \eta_3 = 1.84 \pm 0.20 \ , \tag{29c}$$

$T_\infty = 10^4$ was used.

From the scaling coefficients, one may conclude that, T_c is closely related to $\widetilde{x}$ rather than to σ_x. This is reasonable, since in fact, the trapping time T_c is when the soliton's kinetic energy decreases to the same magnitude as the random potential energy (as we checked explicitly). The standard derivation on the other hand reflects the variation of position for $t > T_c$.

For very weak disorder $W \lesssim 0.04$ the scaling (27) seems not to be valid. The soliton seems to loose its velocity keeping its mass nearly constant. In particular $T_c \approx 10^5$ for $W = 0.02$.

V. SUMMARY AND CONCLUSIONS

Dynamics of solitons in random potentials was studied in the framework of the Ablowitz-Ladik model [2]. In particular we explored the question when can a soliton be considered as a particle and what are the conditions for trapping of solitons in a random potential. The behavior was classified into three regimes specified by Eq. (17). In the regime $\mu_0 \gg 1$ for short times the approximation (18) holds. In particular μ changes in time resulting in the change of the soliton width. This destroys the semianalytic solution resulting of (18) as is clear from Fig. 1. For $\mu_0 \ll 1$ the soliton spreads very quickly and the potential picture is not appropriate.

The most interesting regime is when $\mu_0 \approx 1$, where the soliton is trapped and moves as a particle with varying mass. The equality of $F_1 = F_2$ that is demonstrated in Fig. 4 is a strong evidence for the particle nature. The velocity changes its direction at some maxima of the potential (23) as can be seen from Fig. 4(e) and as expected from (24). Better understanding

of the potential $U(t)$ and its relation to the average of the random potential over the profile of the soliton will be left for future studies. Finally we found that T_c, the first time when the velocity changes direction, scales with the strength of the random potential according to (26) and the potential is scaling function of time and the strength of random potential.

ACKNOWLEDGEMENTS

The comments from the referees are well appreciated. Z.-Y. S. acknowledges the support in part at the Technion by a fellowship of the Israel Council for Higher Education. This work was partly supported by the Israel Science Foundation (ISF-1028), by the US-Israel Binational Science Foundation (BSF-2010132), by the USA National Science Foundation (NSF DMS 1201394) and by the Shlomo Kaplansky academic chair.

Appendix A

Refs. [11] show that for an AL model with a perturbation term

$$i\frac{\partial \psi_n}{\partial t} = -(\psi_{n-1} + \psi_{n+1})(1 + |\psi_n|^2) + R_n \ , \tag{A.1}$$

the soliton parameters in (2) in the adiabatic approximation satisfy the following evolution equations

$$\dot{\mu} = \sinh(\mu) \sum_{n=-\infty}^{+\infty} \frac{\cosh[\mu(n-x)]\mathrm{Im}(r_n)}{\cosh[\mu(n+1-x)]\cosh[\mu(n-1-x)]} \ , \tag{A.2a}$$

$$\dot{x} = \frac{2\sinh(\mu)}{\mu}\sin(k) + \frac{\sinh(\mu)}{\mu} \sum_{n=-\infty}^{+\infty} \frac{(n-x)\cosh[\mu(n-x)]\mathrm{Im}(r_n)}{\cosh[\mu(n+1-x)]\cosh[\mu(n-1-x)]} \ , \tag{A.2b}$$

$$\dot{k} = -\sinh(\mu) \sum_{n=-\infty}^{+\infty} \frac{\sinh[\mu(n-x)]\mathrm{Re}(r_n)}{\cosh[\mu(n+1-x)]\cosh[\mu(n-1-x)]} \ , \tag{A.2c}$$

$$\begin{aligned}\dot{\alpha} = {} & 2[\cosh(\mu)\cos(k) + \frac{k}{\mu}\sinh(\mu)\sin(k)] \\ & + \sinh(\mu) \sum_{n=-\infty}^{+\infty} \frac{(n-x)\sinh[\mu(n-x)]\mathrm{Re}(r_n)}{\cosh[\mu(n+1-x)]\cosh[\mu(n-1-x)]} \\ & - \cosh(\mu) \sum_{n=-\infty}^{+\infty} \frac{\cosh[\mu(n-x)]\mathrm{Re}(r_n)}{\cosh[\mu(n+1-x)]\cosh[\mu(n-1-x)]} \\ & + k\frac{\sinh(\mu)}{\mu} \sum_{n=-\infty}^{+\infty} \frac{(n-x)\cosh[\mu(n-x)]\mathrm{Im}(r_n)}{\cosh[\mu(n+1-x)]\cosh[\mu(n-1-x)]} \ ,\end{aligned} \tag{A.2d}$$

where $r_n = R_n \exp[-ik(n-x) - i\alpha]$. For Eq. (8) with the solution form (2) we have

$$r_n = \frac{\varepsilon_n \sinh(\mu)}{\cosh[\mu(n-x)]} \ . \tag{A.3}$$

Substituting (A.3) into (A.2) we obtain Eqs. (18).

Appendix B

In this appendix, we will outline the derivation of Eq. (19). Taking a derivative on both sides of Eq. (5) with respect to t, one obtains

$$\frac{dP}{dt} = i \sum_{n=-\infty}^{+\infty} \left(\frac{\partial \psi_n}{\partial t}\psi_{n+1}^* + \psi_n \frac{\partial \psi_{n+1}^*}{\partial t} - \frac{\partial \psi_n^*}{\partial t}\psi_{n+1} - \psi_n^* \frac{\partial \psi_{n+1}}{\partial t} \right) \ . \tag{B.1}$$

With the help of Eq. (8), we derive the following results

$$\frac{\partial \psi_n}{\partial t} = i[(\psi_{n-1} + \psi_{n+1})(1 + \psi_n \psi_n^*) - \varepsilon_n \psi_n] \ , \tag{B.2a}$$

$$\frac{\partial \psi_n^*}{\partial t} = -i[(\psi_{n-1}^* + \psi_{n+1}^*)(1 + \psi_n \psi_n^*) - \varepsilon_n \psi_n^*] \ , \tag{B.2b}$$

$$\frac{\partial \psi_{n+1}}{\partial t} = i[(\psi_n + \psi_{n+2})(1 + \psi_{n+1} \psi_{n+1}^*) - \varepsilon_{n+1} \psi_{n+1}] \ , \tag{B.2c}$$

$$\frac{\partial \psi_{n+1}^*}{\partial t} = -i[(\psi_n^* + \psi_{n+2}^*)(1 + \psi_{n+1} \psi_{n+1}^*) - \varepsilon_{n+1} \psi_{n+1}^*] \ . \tag{B.2d}$$

Substituting (B.2) into (B.1), after simplification, we obtain

$$\begin{aligned} \frac{dP}{dt} &= \sum_{n=-\infty}^{+\infty} [\varepsilon_n(\psi_n \psi_{n+1}^* + \psi_n^* \psi_{n+1}) - \varepsilon_{n+1}(\psi_n \psi_{n+1}^* + \psi_n^* \psi_{n+1})] \\ &= 2 \sum_{n=-\infty}^{+\infty} \mathrm{Re}(\psi_n \psi_{n+1}^*)(\varepsilon_n - \varepsilon_{n+1}) \ , \end{aligned}$$

that is Eq. (19).

Appendix C

In this appendix, we will discuss the numerical accuracy of our numerical results. We used the 4th-order Runge-Kutta (RK) method to integrate Eq. (8). Although some lower order but more efficient methods, such as the split-step Fourier method, as well as higher order methods, including even the 8th-order RK method, have been cited in the literature [12, 25], we consider the 4th-order RK to have an appropriate balance between accuracy and speed requirements. It is important to note that, we use a moving coordinate system with origin on the soliton and absorbing boundary conditions, which are appropriate for the problem studied here.

In order to test the numerical accuracy, we have performed the following two procedures: first, we varied the step sizes for the 4th-order RK method by orders of magnitude ($\Delta t = 10^{-2} \sim 10^{-4}$), and found the results did not change; second, we employed a different integration scheme, a 2nd-order relaxation scheme developed by Besse [24, 25], and found no significant changes for the soliton behaviors either. Comparison of some typical results, by the 4th-order RK method with different step sizes, and by the Besse method, are presented in Fig. 7. For these reasons numerical results can be trusted.

References

[1] C. Sulem and P.L. Sulem, *The Nonlinear Schrödinger Equation: Self-Focusing and Wave Collapse*, Springer-Verlag (NY) (1999).

[2] M. J. Ablowitz and J. F. Ladik, J. Math. Phys. **16**, 598 (1975); **17**, 1011 (1976).

[3] J. C. Bronski, J. Stat. Phys. **92**, 995 (1998).

[4] E. Akkermans, S. Ghosh, and Z. H. Musslimani, J. Phys. B **41**, 045302 (2008).

[5] Y. V. Kartashov and V. A. Vysloukh, Phys. Rev. E **72**, 026606 (2005).

[6] K. Sacha, C. A. Müller, D. Delande, and J. Zakrzewski, Phys. Rev. Lett. **103**, 210402 (2009).

[7] A. B. Aceves, C. De Angelis, T. Peschel, R. Muschall, F. Lederer, S. Trillo, and S. Wabnitz, Phys. Rev. E **53**, 1172 (1996).

[8] T. Schwartz, G. Bartal, S. Fishman, and M. Segev, Nature **446**, 52 (2007).

[9] A. A. Vakhnenko and Yu. B. Gaididei, Theor. Math. Phys. **68**, 873 (1986).

[10] K. Kundu, Phys. Rev. E **61**, 5839 (2000).

[11] D. Cai, A. R. Bishop, and N. Grønbech-Jensen, Phys. Rev. E **53**, 4131 (1996).

[12] P. G. Kevrekidis, *The Discrete Nonlinear Schrdinger Equation*, Springer-Verlag (Berlin Heidelberg) (2009).

[13] P. G. Kevrekidis, A. Khare, A. Saxena, I. Bena, and A. R. Bishop, Math. Comput. Simulat. **74**, 405 (2007).

[14] S. Fishman, Y. Krivolapov, and A. Soffer, Nonlinearity **25**, R53 (2012).

[15] J. Billy, V. Josse, Z. Zuo, A. Bernard, B. Hambrecht, P. Lugan, D. Clément, L. Sanchez-Palencia, P. Bouyer, and A. Aspect, Nature **453**, 891 (2008).

[16] F. G. Bass, Yu. S. Kivshar, V. V. Konotop, and Yu. A. Sinitsyn, Phys. Rep. **157**, 63 (1988).

[17] S. A. Gredeskul and Yu. S. Kivshar, Phys. Rep. **216**, 1 (1992).

[18] J. C. Bronski, J. Nonlin. Sci. **8**, 161 (1998).

[19] J. Garnier, SIAM J. Appl. Math. **58**, 1969 (1998).

[20] J. Garnier, Phys. Rev. E **63**, 026608 (2001).

[21] R. Franzosi, R. Livi, G.L. Oppo, and A. Politi, Nonlinearity **24**, R89 (2011).

[22] M. Mochol, M. Płodzień, and K. Sacha, Phys. Rev. A **85**, 023627 (2012).

[23] C. A. Müller, Appl. Phys. B **102**, 459 (2011).

[24] C. Besse, SIAM J. Numer. Anal. **42**, 934 (2004).

[25] X. Antoine, W. Bao, and C. Besse, Comput. Phys. Commun. **184**, 2621 (2013).

Figure captions and figures

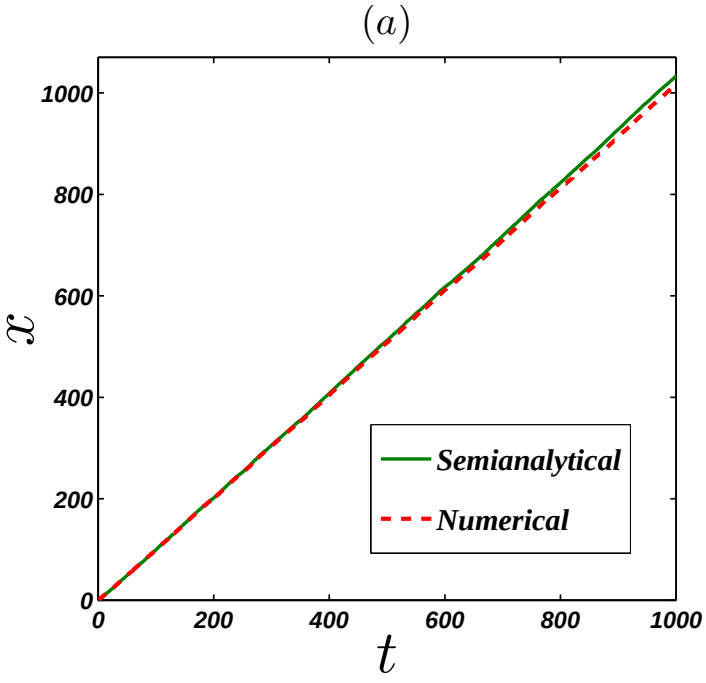

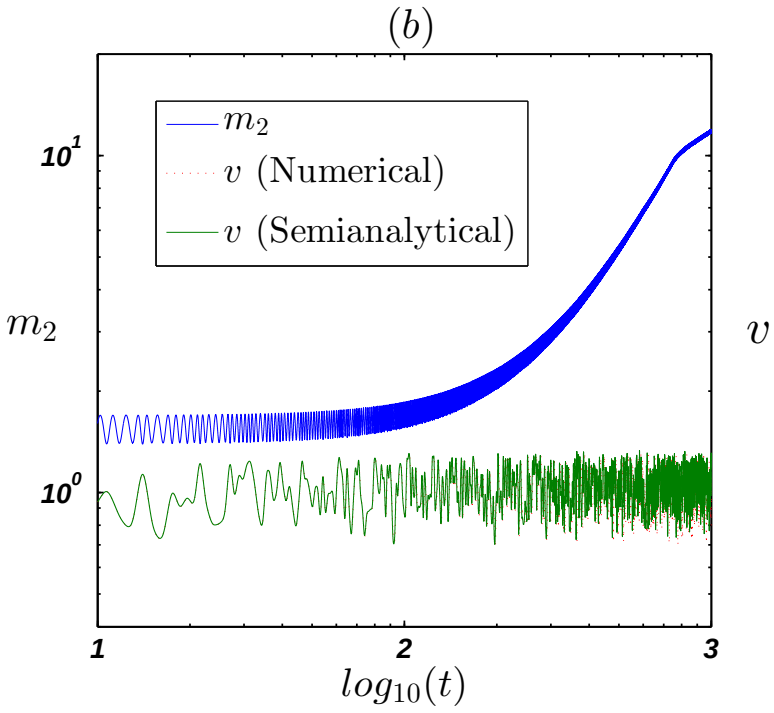

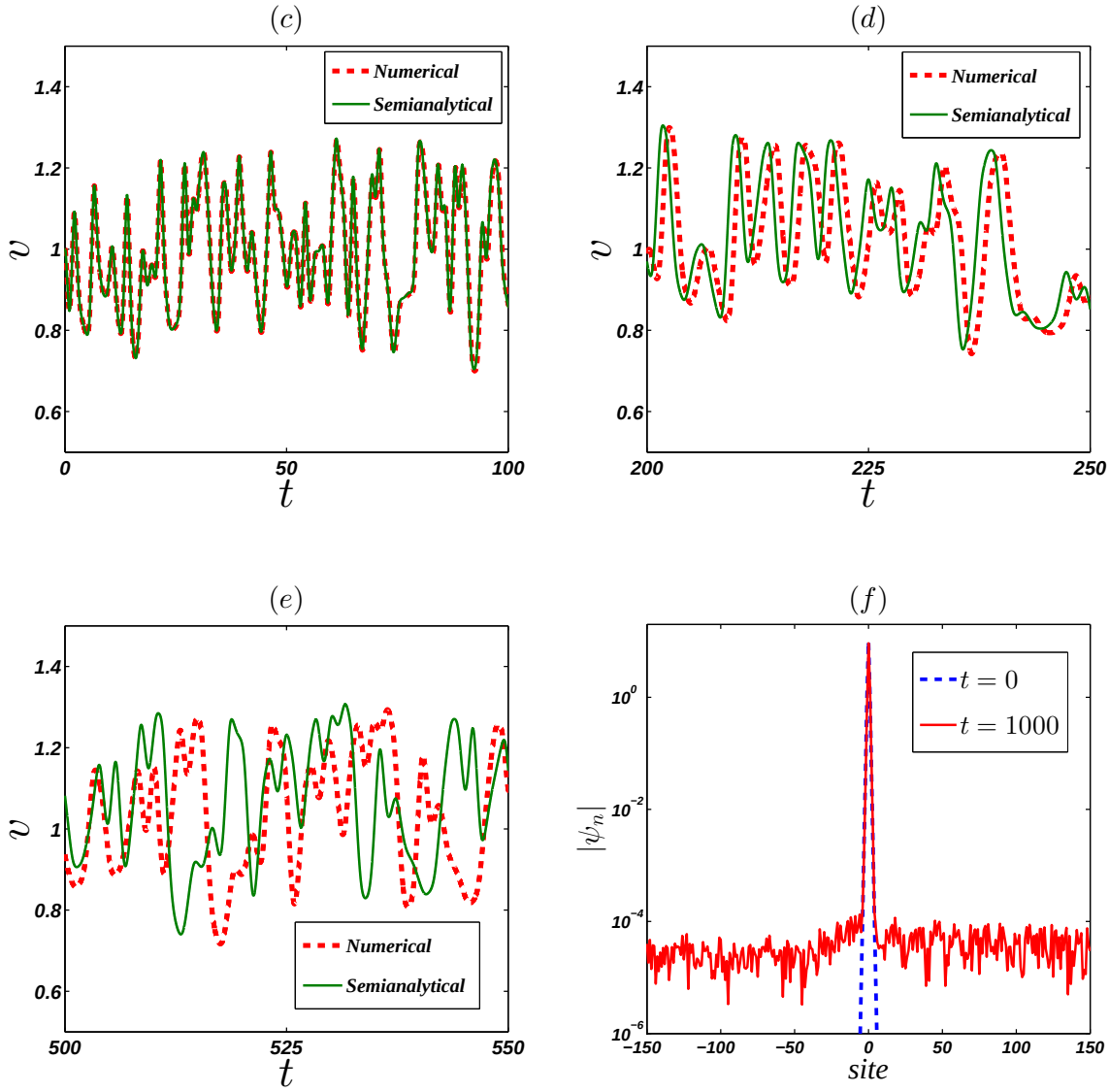

FIGURE 1: (Color online) AL soliton acceleration by one specific realization of random potential [$\mu_0 = 3$, $v(t = 0) = 1$, and $W = 0.1$]. (a) Comparison of the center of mass between the semianalytical (solid green line) and numerical (dashed red line) results. (b) Comparison of the semianalytical (lower solid green line) and numerical (lower dashed red line) velocities, and the second moment m_2 (upper solid blue line). (c)-(e) Zoomed views of the velocity comparison in three different time intervals. (f) The soliton profiles at $t = 0$ (dashed blue line) and $t = 1000$ (solid red line). Note that the site coordinate is fixed on the center of mass.

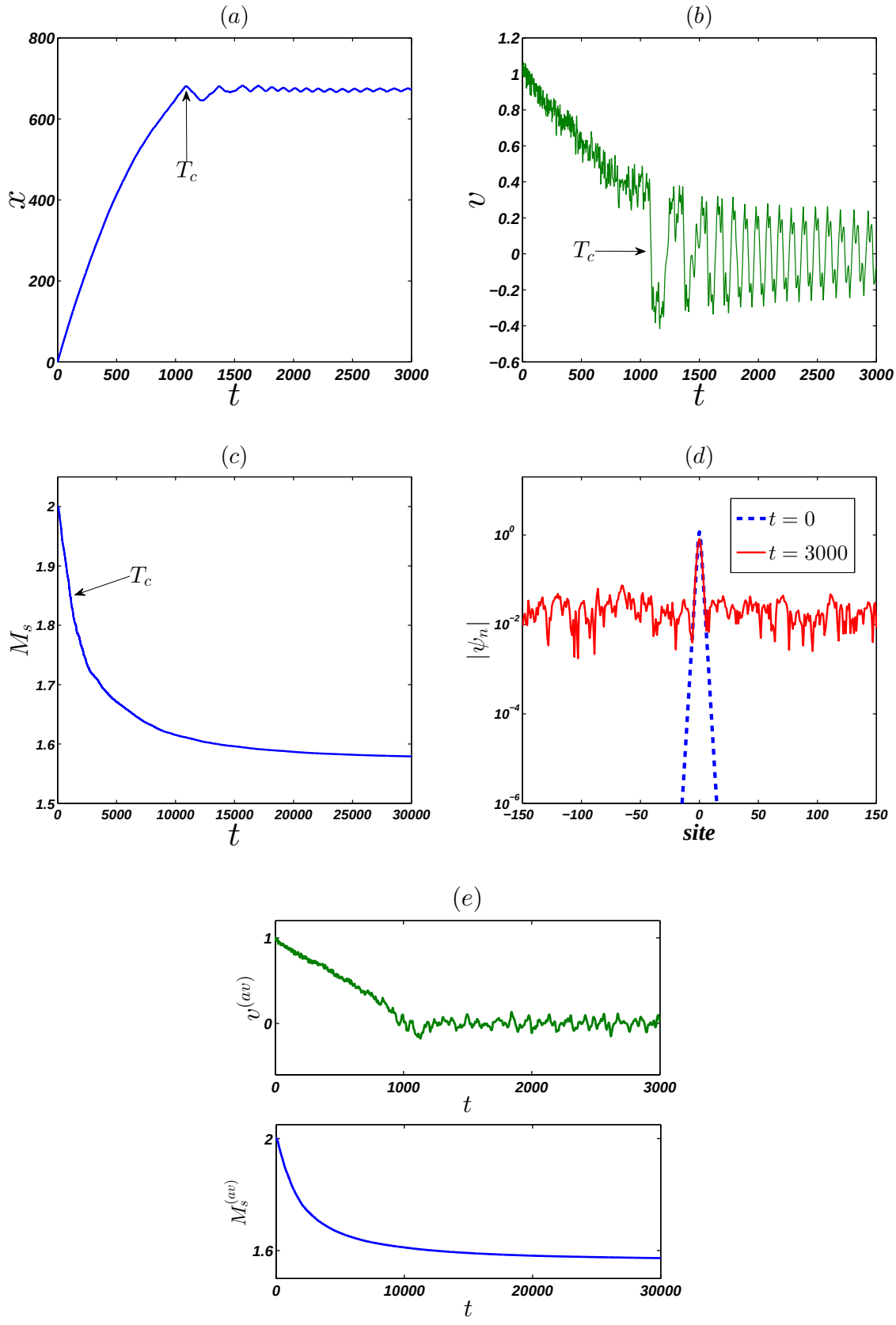

FIGURE 2: (Color online) AL soliton trapping by one realization of random potential [$\mu_0 = 1$, $v(t = 0) = 1$, and $W = 0.1$]. (a) Center of mass x [Eq. (12)] as function of time t. (b) The soliton velocity v [Eq. (14)] as function of time t. (c) The mass M_s [Eq. (11)] as function of time t. (d) The soliton profiles at $t = 0$ (dashed blue line) and $t = 3000$ (solid red line). (e) $v^{(av)}$ and $M_s^{(av)}$ as function of time t (the averaging is performed over 12 realizations).

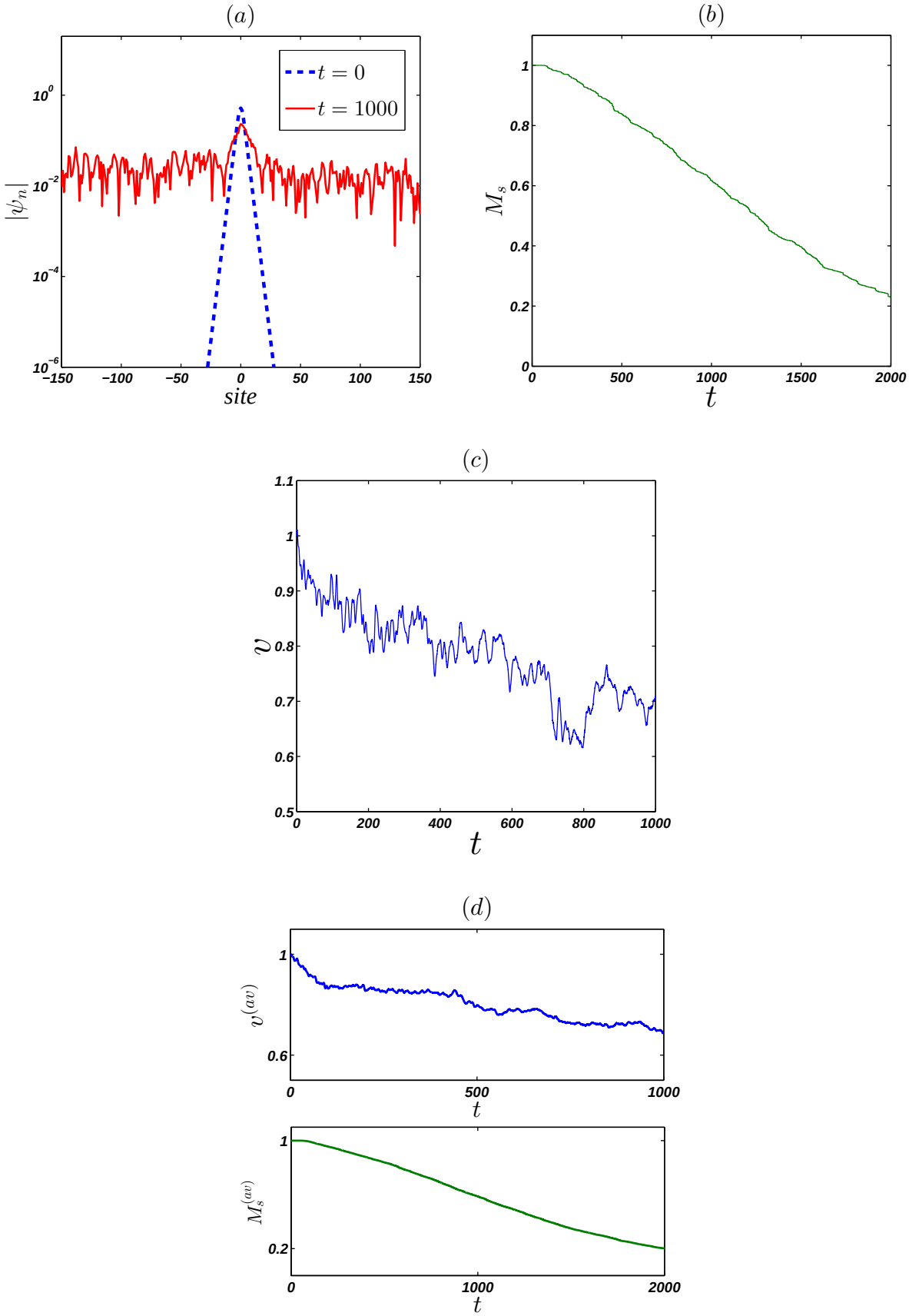

FIGURE 3: (Color online) AL soliton propagation in one realization of random potential [$\mu_0 = 0.5$, $v(t = 0) = 1$, and $W = 0.1$]. (a) The soliton profiles at $t = 0$ (dashed blue line) and $t = 1000$ (solid red line). (b) The mass M_s [Eq. (11)] as function of time t. (c) The soliton velocity v [Eq. (14)] as function of time t. (d) $v^{(av)}$ and $M_s^{(av)}$ as function of time t (the averaging is performed over 12 realizations).

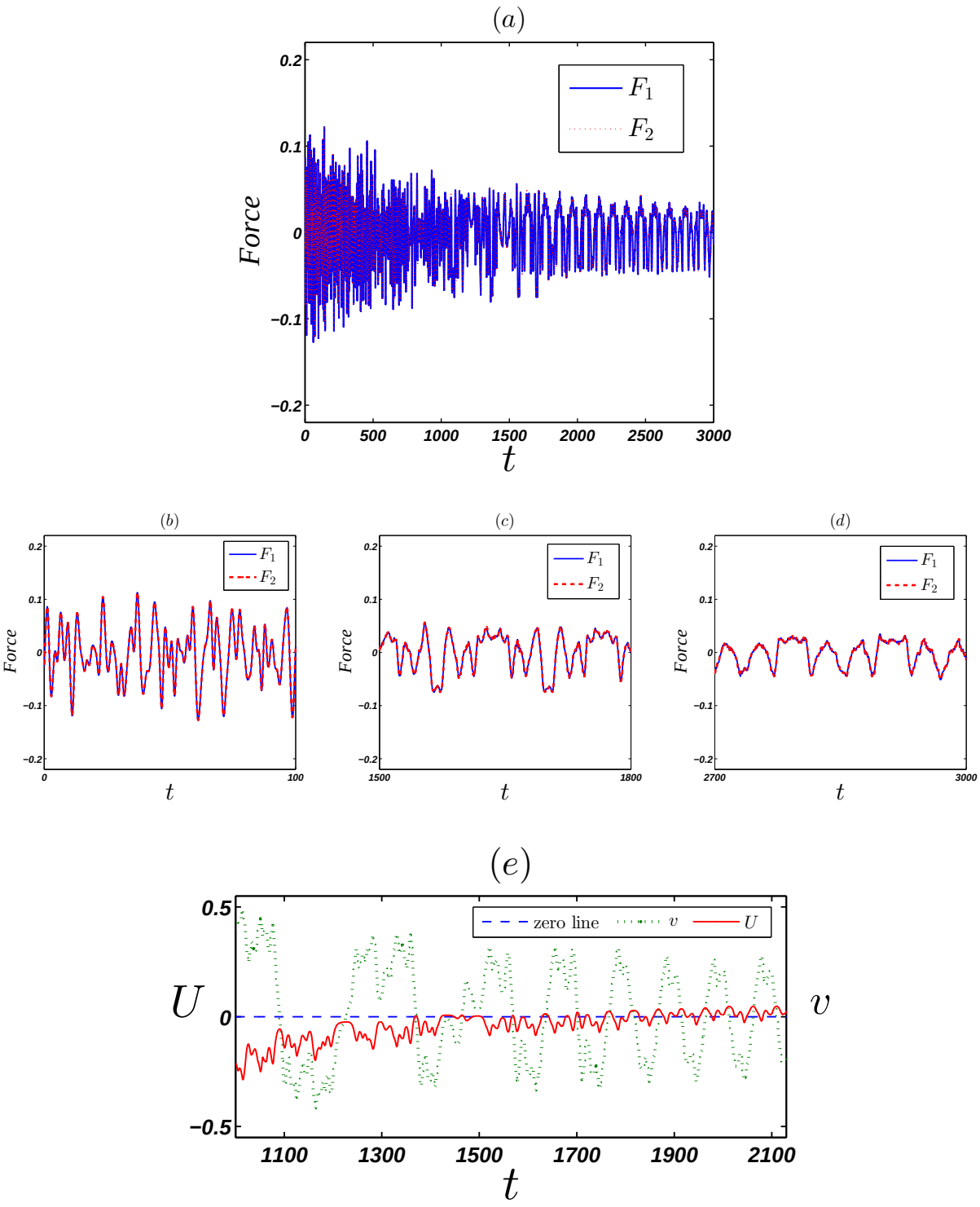

FIGURE 4: (Color online) (a) Comparison of the two forces F_1 [Eq. (21)] (solid blue line) and F_2 [Eq. (22)] (dashed red line) with the soliton parameters and random potential the same as those in Figs. 2(a) and (b). (b)-(d) Zoomed views of the panel (a) for three different time intervals. (e) The effective potential U (solid red line) and soliton velocity v (dotted green line) after the soliton's first reflection ($T_c \approx 1100$).

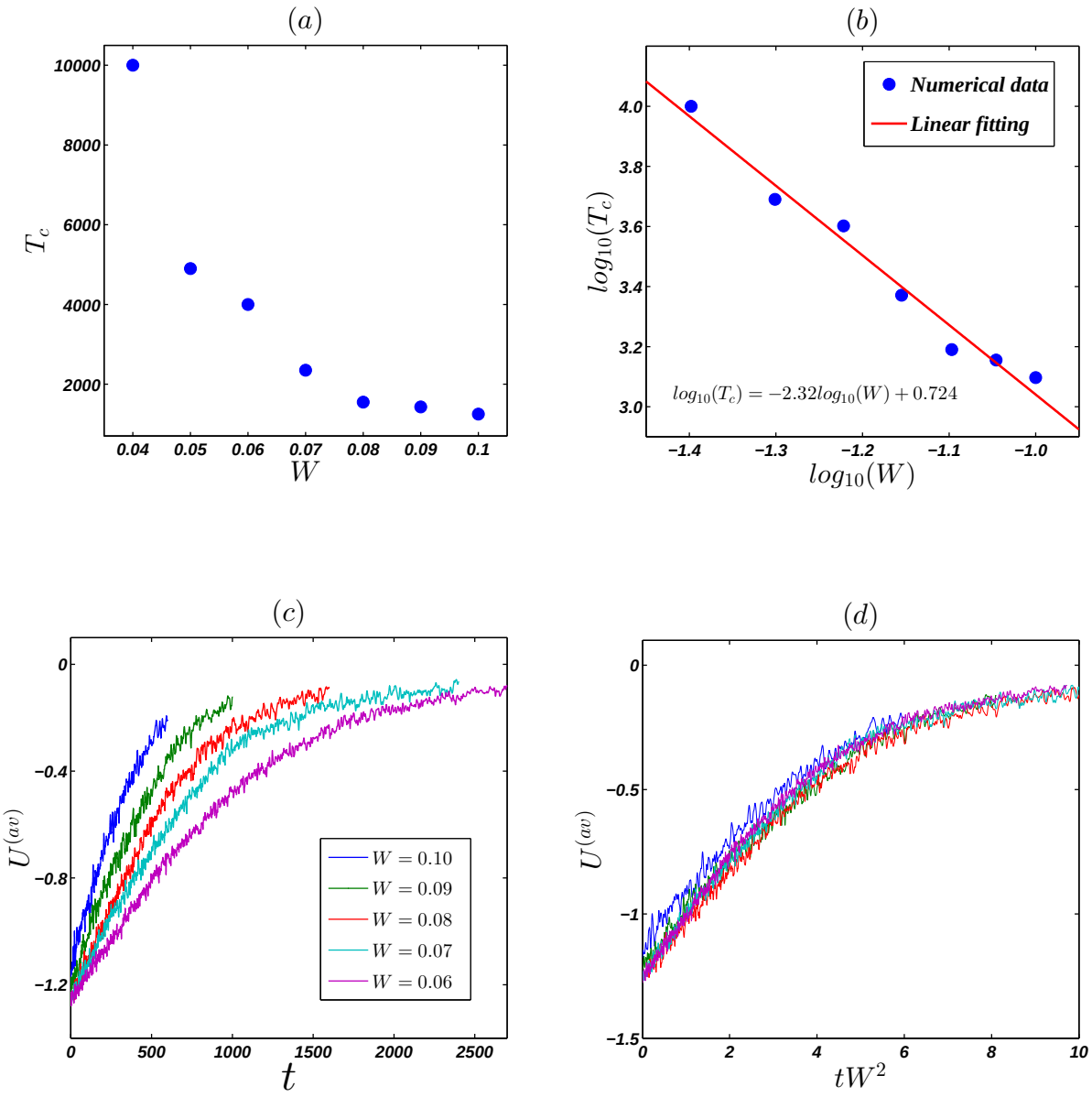

FIGURE 5: (Color online) (a) T_c as function of W. The random potentials are constructed of one realization of random numbers in $[-1, 1]$, multiplied by different strength $W/2$. (b) Linear fit of the data (logarithm forms of variables) in (a). (c) $U^{(av)}$ as function of t and W (the lines from the left to right accord to W from 0.10 to 0.06). (d) $U^{(av)}$ as a function of the scaling variable tW^2.

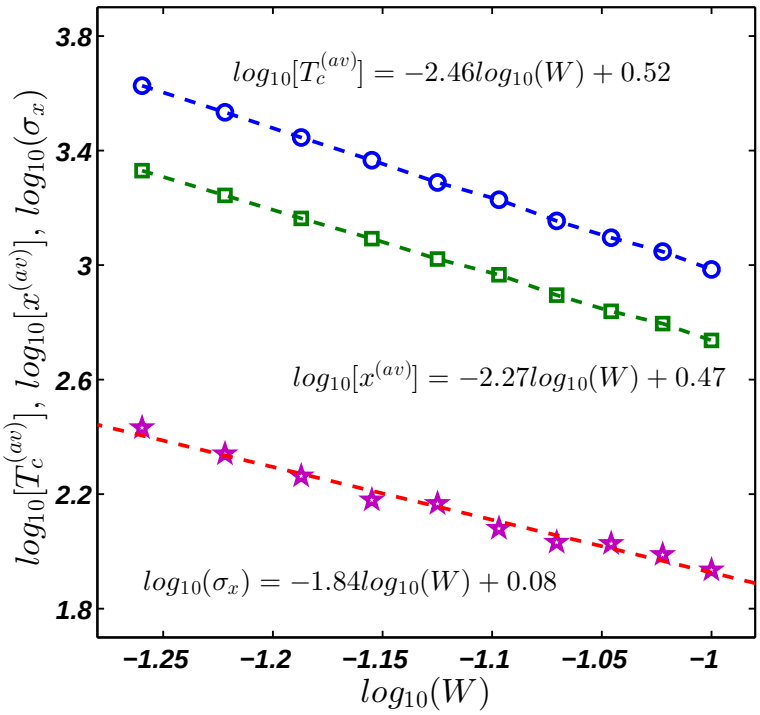

FIGURE 6: (Color online) $T_c^{(av)}$ (blue circles), $x^{(av)}$ (green squares), and σ_x (red stars) as functions of W (linear fit of the logarithm of variables). The averaging is carried out over 250 realizations of random potential. The initial soliton parameters are $\mu_0 = 1$ and $v(t = 0) = 1$.

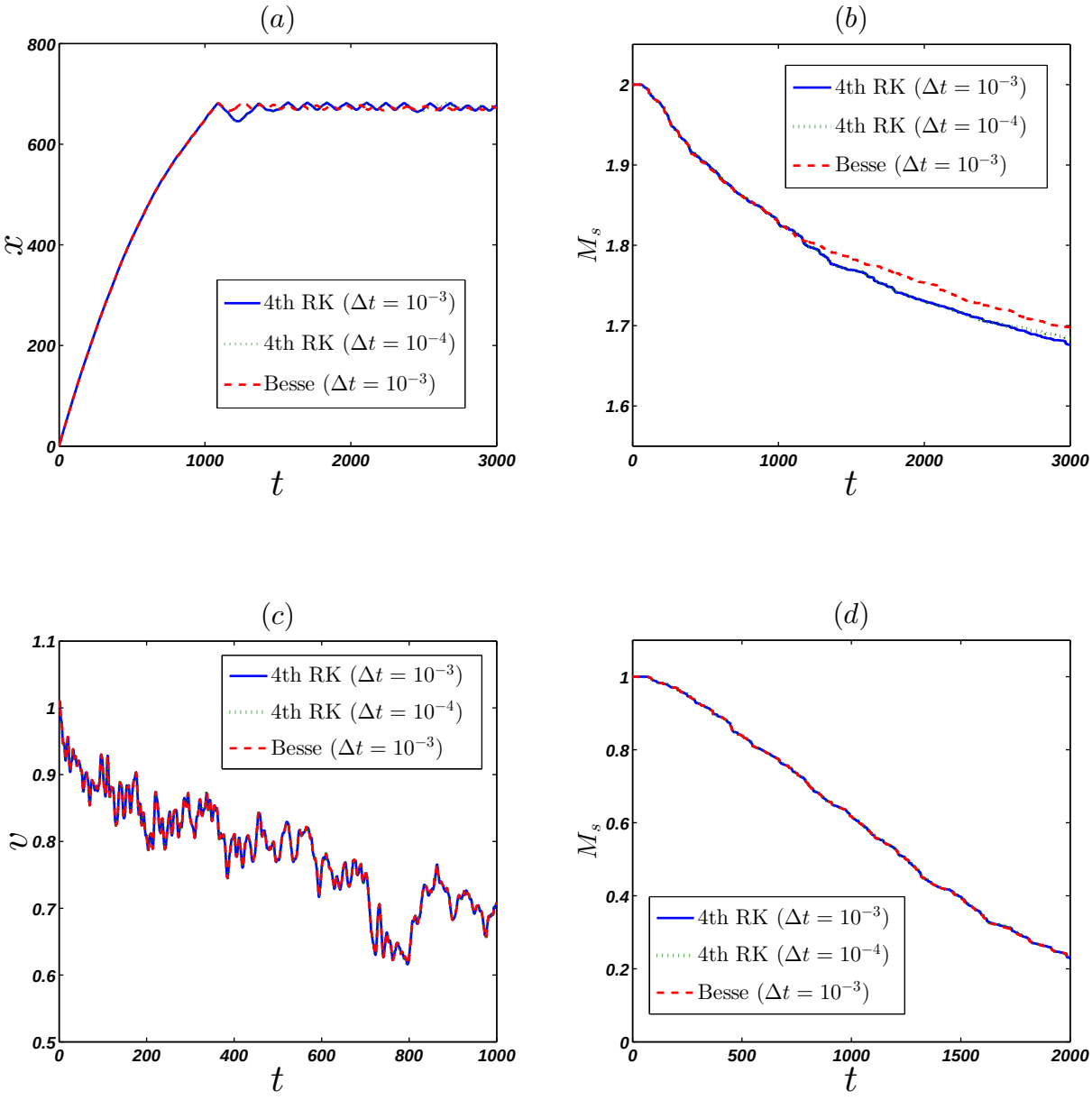

FIGURE 7: (Color online) Comparison of the typical results, as for parameters of Figs. 2 and 3, integrating on Eq. (8) by the 4th-order Runge-Kutta method with different step sizes [$\Delta t = 10^{-3}$ (solid blue line) and $\Delta t = 10^{-4}$ (dotted green line)] and the Besse method with $\Delta t = 10^{-3}$ (dashed red line). (a,b) $\mu_0 = 1$, $v(t = 0) = 1$, and $W = 0.1$ used in Fig. 2 with $\Delta t = 10^{-3}$; (c,d) $\mu_0 = 0.5$, $v(t = 0) = 1$, and $W = 0.1$ used in Fig. 3 with $\Delta t = 10^{-3}$. The RK results of $\Delta t = 10^{-2}$ look similar.